Journal of Power Sources 196 (2011) 10652–10657

Contents lists available at SciVerse ScienceDirect

Journal of Power Sources

journal homepage: www.elsevier.com/locate/jpowsour

Aqueous-phase reforming of n-BuOH over Ni/Al_2O_3 and Ni/CeO_2 catalysts

B. Roy, H. Sullivan, C.A. Leclerc*

Department of Chemical Engineering, New Mexico Institute of Technology, Socorro, NM 87801, United States

ARTICLE INFO

Article history:
Received 30 June 2011
Received in revised form 22 August 2011
Accepted 22 August 2011
Available online 27 August 2011

Keywords:
Hydrogen
Aqueous phase reforming
Bio-butanol
Nickel

ABSTRACT

The aqueous-phase reforming (APR) of n-butanol (n-BuOH) over Ni(20 wt%) loaded Al_2O_3 and CeO_2 catalysts has been studied in this paper. Over 100 h of run time, the Ni/Al_2O_3 catalyst showed significant deactivation compared to the Ni/CeO_2 catalyst, both in terms of production rates and the selectivity to H_2 and CO_2. The Ni/CeO_2 catalyst demonstrated higher selectivity for H_2 and CO_2, lower selectivity to alkanes, and a lower amount of C in the liquid phase compared to the Ni/Al_2O_3 sample. For the Ni/Al_2O_3 catalyst, the selectivity to CO increased with temperature, while the Ni/CeO_2 catalyst produced no CO. For the Ni/CeO_2 catalyst, the activation energies for H_2 and CO_2 production were 146 and 169 kJ mol^{-1}, while for the Ni/Al_2O_3 catalyst these activation energies were 158 and 175 kJ mol^{-1}, respectively. The difference of the active metal dispersion on Al_2O_3 and CeO_2 supports, as measured from H_2-pulse chemisorption was not significant. This indicates deposition of carbon on the catalyst as a likely cause of lower activity of the Ni/Al_2O_3 catalyst. It is unlikely that carbon would build up on the Ni/CeO_2 catalyst due to higher oxygen mobility in the Ni doped non-stoichiometric CeO_2 lattice. Based on the products formed, the proposed primary reaction pathway is the dehydrogenation of n-BuOH to butaldehyde followed by decarbonylation to propane. The propane then partially breaks down to hydrogen and carbon monoxide through steam reforming, while CO converts to CO_2 mostly through water gas shift. Ethane and methane are formed via Fischer–Tropsch reactions of CO/CO_2 with H_2.

1. Introduction

Hydrogen can be considered the most environmentally friendly potential fuel for fuel cell applications due to the carbon-free emission it produces. Yet it has the highest energy content per unit weight of all the fuels; three times the energy of the same mass of gasoline. Hydrogen, produced from renewable biomass instead of non-renewable fossil fuel sources, is an alternative source of environmentally clean renewable energy [1]. Recently n-butanol has been considered as a potentially significant source of H_2 due to its higher weight % of H content compared to ethanol or methanol, low vapor pressure, lower flammability, and ease of handling. Additionally, n-BuOH or biobutanol, can be produced by fermentation of sugar beets, sugar cane, corn, wheat, lignocellulosic biomass and aqueous fraction of biomass pyrolysis liquids (bio-oil) [2]. It can also be produced through the non-fermentative pathways with the help of metabolic engineering [3] and from macroalgae or seaweeds [4,5]. There are different methods of producing H_2 from n-BuOH; such as steam reforming [6,7], partial oxidation [8], dry reforming [9]. Wang and Cao studied partial oxidation of BuOH for hydrogen-rich gas production by the Gibbs free energy minimization method. Reaction temperatures between 842 and 927 °C and oxygen-to-butanol molar ratios between 1.6 and 1.7 at ~101 kPa were identified as the optimum reaction conditions under which complete conversion of butanol, 93.07–96.56% yield of hydrogen, and 94.02–97.55% yield of carbon monoxide could be achieved in the absence of coke formation [8,10]. Nahar and Madhani simulated the thermodynamic parameters of butanol steam reformation for the production of hydrogen by using a Gibbs free-energy-minimization method with water to butanol molar feed ratios (WBFR) between 1 and 18, a pressure range of 100–5000 kPa and reaction temperatures from 300 to 900 °C. On the basis of the equilibrium calculations with higher hydrocarbon compounds excluded, the optimal operating conditions obtained were 600–800 °C, 100 kPa and WBFR 9–12 [6].

Compared to these, aqueous phase reforming (APR) is a single step and low temperature (≤250 °C) energy efficient process that produces hydrogen from water-diluted oxygenated hydrocarbons obtained directly from fermentation. The typical operating pressure and low temperature for APR can be helpful for the separation of H_2 and CO_2 from other products that are volatile at atmospheric pressure. Additionally, APR is useful for producing fuel cell grade H_2 with small amounts of CO in a single chemical reactor due to the water–gas shift (WGS) reaction, which is thermodynamically favored at the lower temperature reaction condition [11,12].

* Corresponding author. Tel.: +1 575 835 5412; fax: +1 575 835 5210.
E-mail address: leclerc@nmt.edu (C.A. Leclerc).

0378-7753/$ – see front matter © 2011 Elsevier B.V. All rights reserved.
doi:10.1016/j.jpowsour.2011.08.093

Reaction kinetics studied for aqueous-phase reforming of ethylene glycol over various supported metals indicated that Pt and Pd catalysts are selective for production of H_2 and Pt shows higher catalytic activity, but at a very high cost (~\$1700 oz^{-1} as of 17th October, 2010). This, coupled with the limited availability of Pt, makes it advantageous to develop catalysts based on less expensive metals, such as Ni (~\$10 lb^{-1}) [13,14]. Studies show that in order to achieve high H_2 selectivity on a catalyst for the APR of an oxygenated hydrocarbon, a high C–C bond breaking rate, a low C–O breaking rate, and a low methanation reaction rate on metal, and low acidic catalyst supports are required [1]. For Ni, C–C bond breakage is reported to be high with reasonably good water gas shift activity compared to Co, Pt, Pd, Fe, Ir, and Rh [15–17].

Solution combustion synthesis (SCS) is a fast, simple, and energy efficient technique for the preparation of pure, porous, and small-particle size ceramics generally used as catalysts, phosphors, pigments, etc. [18–20]. We have reported APR of EtOH over alumina supported nano-scale nickel catalysts prepared by a SCS method before [21]. Bimbela et al. reported the steam reforming of n-BuOH over Ni/Al_2O_3 catalyst prepared by a co-precipitation method [7]. This is the first work reporting on the formation of H_2 by APR of n-BuOH.

In this paper, we present results of preliminary study on aqueous-phase reforming of n-BuOH over Ni/CeO_2 and Ni/Al_2O_3 catalysts. Both supports were prepared by a SCS route. The performance of these catalysts has been compared in terms of BuOH conversion, yield and selectivity to the products in gaseous and liquid effluents.

2. Experimental

2.1. Preparation of catalysts

Supports for Ni(20 wt%) loaded catalysts have been prepared by a solution combustion method. The stoichiometric amounts of metal nitrates [$(Al(NO_3)_3{\cdot}9H_2O$, Arcos Inc., >99% for Al_2O_3 and $Ce(NO_3)_3{\cdot}6H_2O$, Arcos Organics, >99% for CeO_2 powders] were mixed thoroughly with glycine ($C_2H_5NO_2$, Fisher, 99.5%) separately by using a mortar and pestle. The mixed mass was transferred to a 270 cc Pyrex crystallization dish and ignited at 400 °C on a hot plate. After initial boiling and frothing, the mixture eventually ignited at one spot, and spread out over the entire dish yielding a voluminous black foam. The collected powder was washed 4–5 times with deionized water ultrasonically to remove excess fuel and un-reacted salt followed by drying at 100 °C in an oven. The dried Al_2O_3 powder was heat treated for 2 h at 600 °C and the appearance of the powder changed from black foam to white powder as residual carbon burned off. The CeO_2 powder was not calcined. The metal was loaded on the SCS powders by the wet impregnation method. The Ni/Al_2O_3 and Ni/CeO_2 catalysts were heat treated at 750 °C for 2 h and 350 °C for 2 h, respectively, in air. These catalysts are called 'fresh' catalysts. The BET and H_2-pulse chemisorption techniques were discussed elaborately in our previous publication [21].

2.2. Catalytic activity

A continuous flow stainless steel reactor (0.625 cm inner diameter and 7.5 cm length) set inside a box furnace with a fixed bed catalyst powder has been used to study the catalytic activity of the powders. The catalyst powders were reduced under 10% H_2–Ar mixture and loaded (0.1–0.5 g) in the reactor in between two layers of quartz wool. The Ni/Al_2O_3 and Ni/CeO_2 catalysts were reduced at 1050 °C for 2 h and 450 °C for 2 h, respectively. The BuOH–H_2O solution was fed in the reactor at a continuous flow rate of 0.02 cc min^{-1} by a syringe pump (Teledyne, D500). The reaction was carried out with UHP N_2 as a condenser sweep gas at different pressures in the temperature range of 185–215 °C.

The products from the reactor passed through a homemade phase separator. The gas collected from the separator was analyzed by a gas chromatograph (Micro GC 3000, Agilent Inc.) with a thermal conductivity detector (TCD) and the liquid product was analyzed by an Agilent 6890N GC with a flame ionization detector (FID).

3. Results

The APR was performed on 5 wt% BuOH–H_2O solution at ~2758 kPa and from 185 to 215 °C. At 185 and 215 °C bubble pressures of 5 wt% BuOH–H_2O are ~1117 and 2096 kPa, respectively. Under these reaction conditions, the partial pressure of product H_2

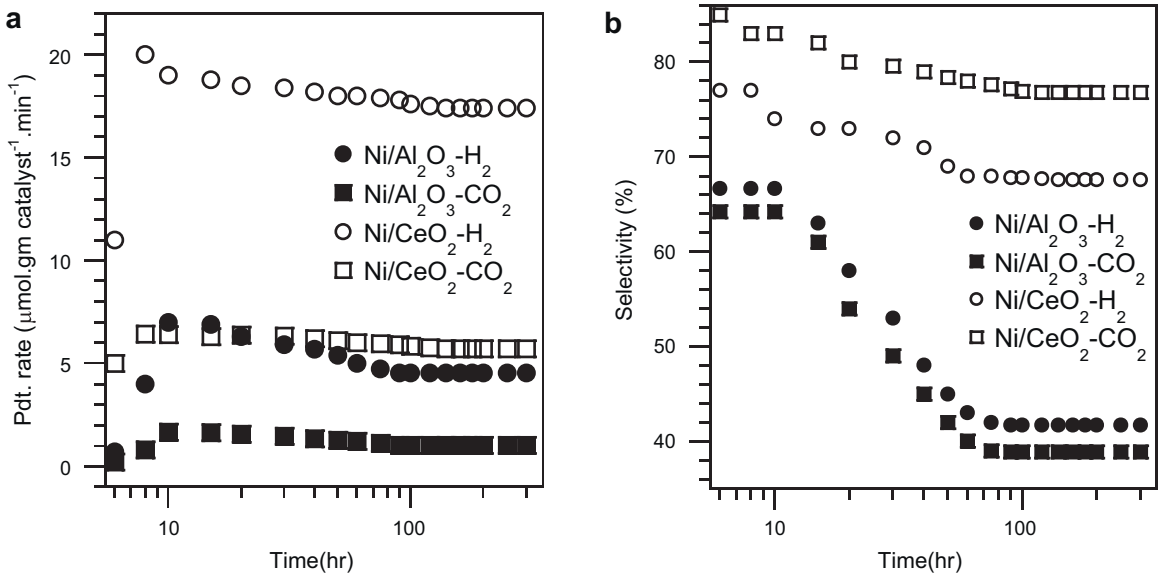

Fig. 1. Change of (a) production rate and (b) selectivity of H_2 and CO_2 as a function of time at 215 °C, 400 psi pressure, and 0.02 cc min^{-1} feed flow rate for aqueous-phase reforming of 5 wt% BuOH using Ni/CeO_2 and Ni/Al_2O_3 catalysts of 20 wt% Ni loading. Initially the catalysts show decrease of H_2 and CO_2 production rate and selectivity and after 100 h of runs both of the catalysts somewhat stabilized.

and CO_2 are maintained almost constant over the range of temperatures. A blank run showed 0.3–0.5% BuOH loss. Analysis of the effluent gas and collected liquid yielded a complete C balance within 1% of the BuOH and H_2O fed. The BuOH conversion increased with increasing temperature, as expected and maintained almost a linear relationship. For Ni/CeO_2 and Ni/Al_2O_3 catalysts the highest conversion was 5.77 and 2.76%, respectively at 215 °C. Although, BuOH conversion on the Ni/CeO_2 catalysts was higher than the Ni/Al_2O_3 catalyst, here we are only reporting low temperature results, where conversion was intentionally restricted to ~5–6% for the kinetic study. Higher temperature studies to investigate high conversion are in progress. The APR effluent gas products were a mixture of H_2, CO_2, CO, and alkanes (C_1–C_3, mostly C_3H_8, with some C_2H_6 and CH_4), while the liquid product was only butaldehyde (C_3H_7CHO). The H_2 selectivity was calculated as the number of moles of H_2 in the effluent gas normalized by the number of moles of H_2 that would be made if each mole of C in the effluent gas had participated in the reforming reaction ideally to give 3 moles of H_2 according to the equation:

$$C_4H_9OH + 7H_2O \leftrightarrows 4CO_2 + 12H_2 \quad (1)$$

The CO_2, CO, and alkanes selectivity has been calculated as

$$S(\%) = \frac{[\text{C in that product}]}{[\text{total C output as gas products}]} \quad (2)$$

Fig. 1 shows the change of (a) production rate and (b) selectivity of H_2 and CO_2 as a function of time at 215 °C. Over 100 h run time for Ni/CeO_2, the production rate of H_2 and CO_2 dropped by 13 and 11%, and the selectivity to H_2 and CO_2 fell 12.2 and 7.5%, respectively. For the Ni/Al_2O_3 catalyst, the production rate of H_2 and CO_2 dropped 41 and 45%, and the selectivity to H_2 and CO_2 dropped by 37.5 and 39.5%, respectively. After the initial decrease, the catalytic activity stabilized for both of the catalysts and the following discussion reflect the results after 100 h run, which is considered to be steady state.

Fig. 2 shows the effect of reaction temperature and support on the selectivity of the gaseous products. The Ni/CeO_2 catalyst produced no CO. The selectivity of H_2, CO_2, and CO (for Ni/Al_2O_3) increased and alkanes decreased with the increase of reactor temperature, in general. For the Ni/Al_2O_3 catalyst, selectivity to CO_2 increased up to 205 °C and then slightly decreased at 215 °C. At 215 °C, the Ni/CeO_2 catalyst had H_2, CO_2, and alkane selectivities of ~67.6, 76.8, and 23.2%, which are ~38 and 49% higher and 54% lower than that of the values obtained by the Ni/Al_2O_3 catalyst, respectively. The selectivity to the type of alkanes is also temperature dependent (Fig. 3). Selectivity to C_3H_8 decreased and lower molecular weight alkanes increased as temperature increased. At 185 °C the Ni/CeO_2 and Ni/Al_2O_3 catalysts showed alkane selectivities of 66.9% and 86.2% for C_3H_8, 9.6 and 13.8% for C_2H_6, and 23.6 and zero % for CH_4, respectively. At 215 °C, for Ni/CeO_2 C_3H_8 and C_2H_6 selectivity decreased to 61.4 and 2.9%, and CH_4 selectivity increased to 35.7%. For Ni/Al_2O_3, the C_3H_8 selectivity decreased to 63%, and the C_2H_6 and CH_4 selectivities increased to 34.5 and 2.35%, respectively. The C% in the liquid effluent decreased as temperature increased but the Ni/CeO_2 catalyst showed a larger change with temperature than the Ni/Al_2O_3 catalyst. For example, as the reactor temperature increased from 185 °C to 215 °C, the rate of decrease of carbon as butaldehyde was 0.156% °C^{-1} and 0.207% °C^{-1} for the Ni/Al_2O_3 and Ni/CeO_2 catalysts, respectively. Bimbela et al. observed very different results for catalytic steam reforming of n-BuOH over Ni/Al_2O_3 catalysts. In the gas phase effluent, only H_2, CO_2, and CO were produced with negligible amount of CH_4 and ethylene. Ethylene was nonexistent at 550 °C, detected in very small amount at 650 °C, and then became significant at 750 °C. In terms of gas compositions, the H_2 and CO_2 content decreased with increasing temperatures while CO, CH_4 and ethylene increased [7]. The composition of liquid effluent was not reported. The higher feed flow rate (0.23 vs. 0.1 cc min^{-1}) and higher reaction temperature might explain the difference of the distribution of the product compounds.

The particle size (d_{BET}) of the fresh Ni/CeO_2 catalyst calculated from the BET surface area S_{BET} (according to the relation $d_{BET} = 6/\rho S_{BET}$, where, ρ = theoretical density [~4 g cc^{-1} for γ-Al_2O_3,

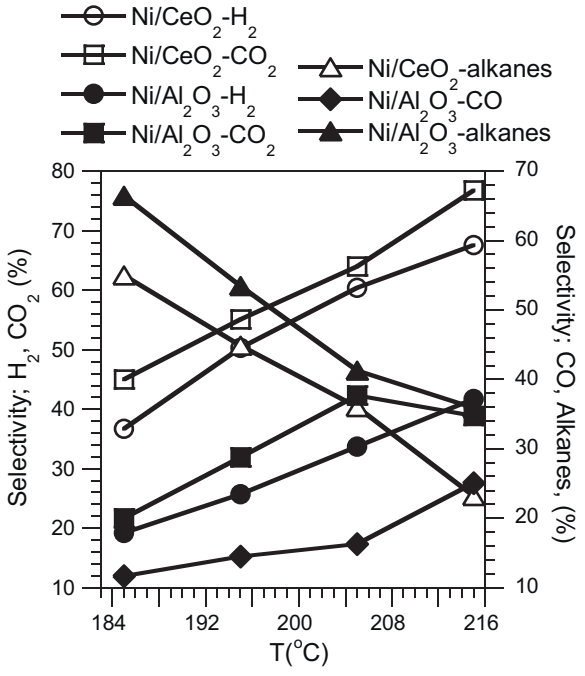

Fig. 2. Selectivity of the gases; H_2, CO_2, alkanes, and CO as a function of temperature for aqueous-phase reforming of 5 wt% BuOH using Ni/CeO_2 and Ni/Al_2O_3 catalysts of 20 wt% Ni loading at 400 psi pressure and 0.02 cc min^{-1} feed flow rate.

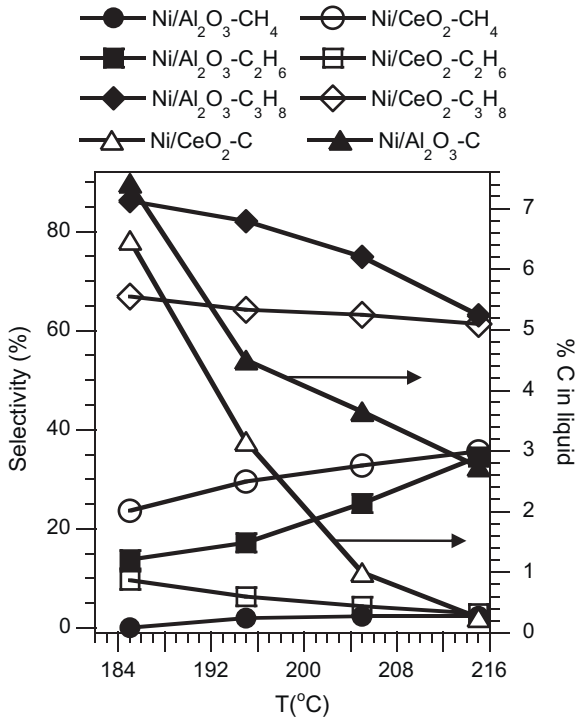

Fig. 3. Steady state selectivity of the alkanes and % of C in liquid as a function of temperature for aqueous-phase reforming of 5 wt% BuOH using Ni/CeO_2 and Ni/Al_2O_3 catalysts of 20 wt% Ni loading at 400 psi pressure and 0.02 cc min^{-1} feed flow rate.

Table 1
BET surface area and H_2-chemisorption results for the catalysts.

Catalysts	S_{BET} ($m^2\,g^{-1}$)			H_2-chemisorption					
	Fresh	Reduced	Used	Metal surface area ($m^2\,g^{-1}$)		Metal dispersion (%)		Active metal particle size (nm)	
				Reduced	Used	Reduced	Used	Reduced	Used
Ni/CeO_2	130	118	110	37.5	32.9	5.6	4.9	18.0	20.5
Ni/Al_2O_3	178	107	78	27.0	24.0	4.2	3.6	25.0	28.0

~7.2 g cc^{-1} for CeO_2, and 6.67 g cc^{-1} for NiO]), was smaller than that of the Ni/Al_2O_3 catalyst (Table 1). This indicates the presence of relatively smaller CeO_2 particles in the Ni/CeO_2 catalyst. During the reduction stage and after using in the reactor, the particle size of both of the catalysts grew larger, but the growth was more severe for the Ni/Al_2O_3 catalyst due to the higher reduction temperature. In our previous work, it has been shown that the Ni/Al_2O_3 catalysts prepared on SCS Al_2O_3 powder, both in fresh and reduced stages, could be indexed as spinel $NiAl_2O_4$ and cubic γ-Al_2O_3 [22]. After using in the reactor, the catalyst support was transformed to boehmite, the high surface area hydrated γ-Al_2O_3 phase. This backward transformation is caused by the hydrothermal high temperature, high pressure conditions of the reactor and has been reported by others previously [23]. The H_2-chemisorption results revealed slightly higher metal dispersion and metal surface area, and lower active metal particle size for the Ni/CeO_2 catalyst compared to the Ni/Al_2O_3 sample, both as reduced and used conditions.

The effect of the reaction temperature and support on the production rate of H_2 and CO_2 per active metal site (turnover frequencies – TOF; calculated on the basis of surface metal dispersion obtained from irreversible H_2-pulse chemisorptions of fresh samples) is shown in Fig. 4. At 215 °C, for the Ni/CeO_2 sample, the TOF values of H_2 and CO_2 were $1.7 \times 10^{-3}\,s^{-1}$ and $5.6 \times 10^{-4}\,s^{-1}$, while for Ni/Al_2O_3 sample these values were $5.3 \times 10^{-4}\,s^{-1}$ and $1.2 \times 10^{-4}\,s^{-1}$, respectively. For the Ni/CeO_2 and Ni/Al_2O_3 catalysts, the activation energy (E_a) values for H_2 production were 146 and ~169 kJ mol^{-1}, respectively, and for CO_2 production the E_a values were 158 and ~175 kJ mol^{-1}, respectively. This is as good as the reported E_a (~140 kJ mol^{-1}) for vapor phase oxidation of n-BuOH over Pt/Al_2O_3 [24]. The E_a values for BuOH conversion were 109 and 121 kJ mol^{-1} for $Ni/CeO_2$and Ni/Al_2O_3, respectively.

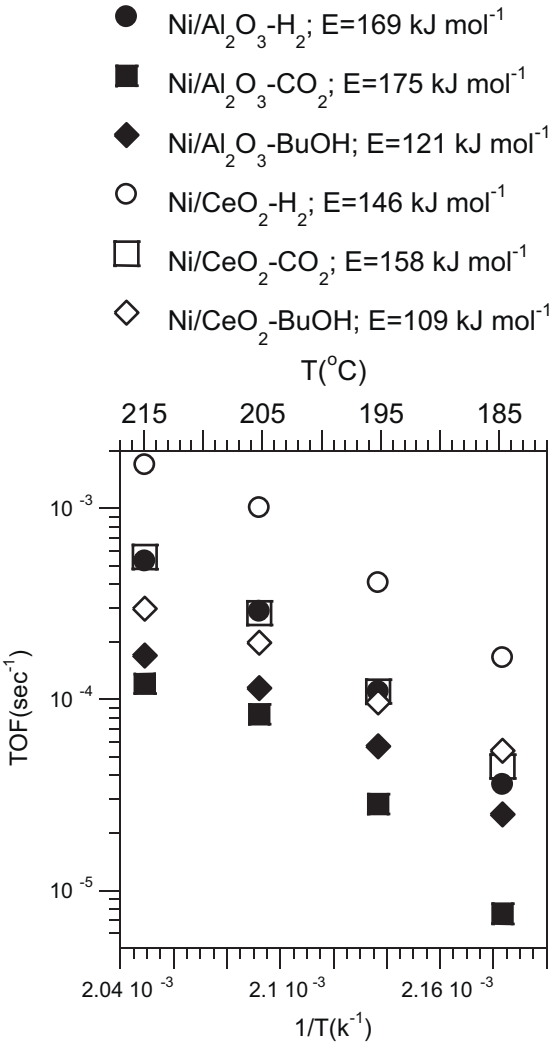

Fig. 4. Variation of turnover frequencies (TOF) for H_2 andCO_2 production and for n-BuOH conversion with 1/T (X1 axis) and temperature (X2 axis) for aqueous-phase reforming of 5 wt% BuOH at 400 psi pressure and 0.02 cc min^{-1} feed flow rate. The solid lines show best fits through the data and slope of the TOF vs.1/T used for calculating activation energy for H_2 and CO_2 production and for n-BuOH conversion.

4. Discussion

4.1. Reaction pathway

A possible reaction pathway which can be drawn based on the products is schematically shown in Fig. 5 and described as follows:

Reaction step 1: dehydrogenation leading to formation of butaldehyde

$$C_4H_9OH \leftrightarrows C_3H_7CHO + H_2 \quad (3)$$

Reaction step 2: breaking of C–C bond according to the equation

$$C_3H_7CHO \leftrightarrows C_3H_8 + CO \quad (4)$$

Reaction step 3: CO can make CO_2 via WGSR

$$CO + H_2O \leftrightarrows CO_2 + H_2 \quad (5)$$

Reaction steps 4 and 7: steam reforming of propane/methane/ethane to CO/H_2

$$C_3H_8 + 3H_2O \leftrightarrows 3CO + 7H_2 \quad (6)$$

$$C_2H_6 + 2H_2O \leftrightarrows 2CO + 5H_2 \quad (7)$$

$$CH_4 + H_2O \leftrightarrows CO + 3H_2 \quad (8)$$

Reaction steps 5 and 6: formation of methane and ethane via Fischer–Tropsch reactions

$$nCO_2 + (3n+1)H_2 \leftrightarrows C_nH_{2n+2} + 2nH_2O \quad (9)$$

$$nCO + (2n+1)H_2 \leftrightarrows C_nH_{2n+2} + nH_2O \quad (10)$$

Steps 1 and 2 are based on the production of butaldehyde and propane without the presence of other C_3–C_4 hydrocarbons. Due to the large presence of CO_2, it is likely that the CO_2 is formed from WGSR due to the large excess of water in the feed. Steps 4 and 7 are likely routes to CO/H_2 though it is possible that butaldehyde and butanol could be steam reformed directly to these products.

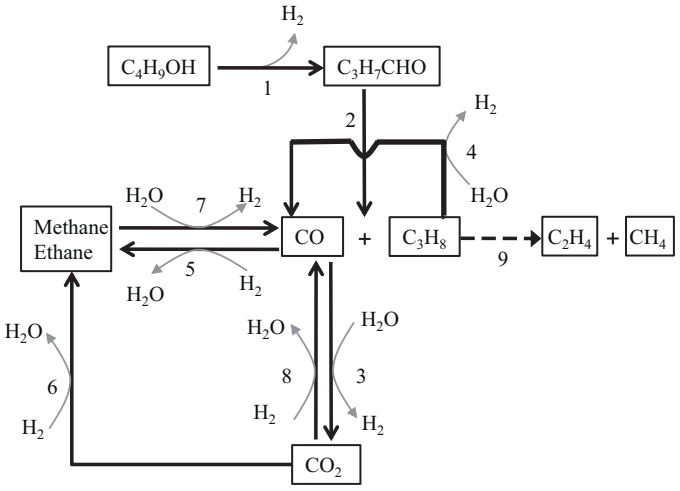

Fig. 5. Possible reaction steps for aqueous phase reforming of n-BuOH on the catalysts.

It is unknown whether or not steam reforming of butanol would go through a butaldehyde or propane intermediate thus we cannot rule out multiple paths to CO/H_2. Steps 5 and 6 explain the presence of methane and ethane in the product stream. It could be possible that methane is formed by step 9, but as we did not see any alkenes, that route is not considered as a probable step and is shown as a dotted line. Low temperature APR treatment has a general tendency of lowering H_2 and CO_2 selectivity by increasing thermodynamically stable alkane and water production by methanation and Fischer–Tropsch reactions [1,11]. It is also possible that any of these small hydrocarbons could be steam reformed to hydrogen and carbon monoxide due to the large excess of water.

In summary, it appears that the butanol is initially dehydrogenated to butaldehyde followed by decarbonylation to propane. The propane then breaks down to hydrogen and carbon monoxide through steam reforming. It is also likely that CO_2 is formed mostly from WGS. It is not clear that the butanol steam reforming is independent of propane steam reforming, i.e. propane may be an intermediate of butanol steam reforming. It is also not clear exactly how C_1–C_2 alkanes are formed whether it is from FT or methanation or decomposition of propane.

4.2. Effect of the support: Al_2O_3 vs. CeO_2

In our previous work on APR of EtOH, 10 wt% Ni loaded Al_2O_3 catalysts showed significant activity at much lower temperature [22]. At the reaction conditions of ~2068 kPa, 155 °C, and 0.02 cc min^{-1} flow rate for 10 wt% EtOH feed, the Ni(10%)/Al_2O_3 catalysts prepared on SCS Al_2O_3 showed EtOH conversion of 5.64%, CO_2 selectivity of 71%, H_2 selectivity of 84%, and alkanes selectivity of 29%, respectively. The activation energies for H_2 and CO_2 production were within the window of 153–167 kJ mol^{-1} and 155–171 kJ mol^{-1} depending on the method of catalyst preparation SCS or sol–gel. Metal catalysts with lower dispersion had a tendency of increasing activation energy. The H_2 and CO_2 selectivities increased and the alkane selectivity decreased with increasing temperature, while no CO was detected for the SCS Ni(10%)/Al_2O_3 catalysts. The same trend was observed for the APR of BuOH over Ni/CeO_2 catalyst. In contrast, the Ni/Al_2O_3 catalyst not only demonstrated a lower BuOH conversion rate, but the production and selectivity of CO (with H_2) also increased with increasing temperature. The total alkanes (smaller C alkanes increased) decreased and CO_2 increased as temperature increased, but above 205 °C selectivity to CO_2 decreased. These indicate that for the Ni/CeO_2 catalyst, the rate of partial reforming of n-BuOH (Eqs. (3) and (4)) and WGSR (Eq. (5); very import aspect of APR) were dominating the system, but for Ni/Al_2O_3 catalysts only part of the CO undergoes WGSR indicating that WGSR is slower with the alumina support as opposed to the ceria support, which has been documented in the literature [25,26].

Additionally, after 300 h of APR of n-BuOH, the Ni/Al_2O_3 catalyst showed significant deactivation, although according to the chemisorption results, growth of the active metal particles was not severe. Compared to that, after using at 140–225 °C and 552–2758 kPa continuously for 250 h for APR of EtOH, the SCS and sol–gel derived Ni(10%)/Al_2O_3 catalysts showed no significant sign of deactivation, and after 300 h of use, deactivation (assessed from H_2 production and EtOH conversion) of the SG and SCS catalysts were only ~13% and ~5%, respectively. These facts indicate that deposition of carbonaceous material on the catalyst surface is the likely cause of deactivation rather changes to the catalyst itself. Bimbela et al. reported massive deposition of carbonaceous filaments on the Ni/Al_2O_3 catalyst caused by steam reforming of 1 g n-BuOH per gm catalyst [7]. While the particle size of the active metal phase on the CeO_2 support is only ~28% smaller than that on the Al_2O_3 support, the difference of the activities in these two catalysts can be attributed to the functional differences of the supports. CeO_2 is a non-stoichiometric oxide support with a fluorite structure known for its interesting redox property giving high oxygen mobility through the lattice:

$$2CeO_2 \leftrightarrow Ce_2O_3 + V_O^{\bullet\bullet} + O_O^X + 2e' \quad (11)$$

Ceria is able to change reversibly from Ce_{IV} under oxidizing conditions to Ce_{III} under reducing conditions. Oxygen atoms in CeO_2 are very mobile and leave the ceria lattice easily, giving rise to a large variety of non-stoichiometric oxides with the two limiting cases CeO_2 and Ce_2O_3. Ni doping in CeO_2 can create oxygen vacancies as follows [27–31]:

$$NiO \overset{CeO_2}{\Leftrightarrow} Ni_{Ce}'' + V_O^{\bullet\bullet} + O_O^X \quad (12)$$

On the other hand Al_2O_3 is a stoichiometric oxide showing stability over a wide range of partial oxygen pressure from a very low partial oxygen pressure [32].

5. Conclusions

These results demonstrate that APR can be useful to make H_2 from n-butanol. The Ni/CeO_2 catalyst prepared on the SCS CeO_2 powder showed a higher amount of C in gas phase, higher selectivity for H_2 and CO_2, and lower selectivity to alkanes compared to the Ni/Al_2O_3 sample. The CeO_2 based catalyst produced no CO but the Al_2O_3 supported catalyst produced a significant amount of CO. CeO_2 allows for high oxygen mobility through the lattice. Ni doping increases oxygen vacancy in the CeO_2 lattice. These two factors most probably enhance the oxidation capability of the Ni/CeO_2 catalyst compared to Ni/Al_2O_3 catalyst.

Based on the product distribution, butanol is dehydrogenated to the aldehyde as a primary step followed by decarbonylation of the aldehyde to propane. The propane is likely reformed to carbon monoxide and hydrogen. The WGSR also plays an important role in eliminating CO as would be expected in the excess water environment.

The elaborate characterizations in order to explore mechanisms of steam reforming and APR of n-BuOH over Ni/CeO_2 and Ni/Al_2O_3 catalysts at different temperatures, pressures, feed flow rates, and feed concentrations are currently under investigation.

Acknowledgements

The authors gratefully thank the Department of Energy (award number DE-FC2606NT42854) and Department of Energy Experimental Program to Stimulate Competitive Research (DOE-EPSCoR award number DE-FG02-08ER46530) for the financial support of this research.

References

[1] R.R. Davda, J.W. Shabaker, G.W. Huber, R.D. Cortright, J.A. Dumesic, Appl. Catal. B 56 (2005) 171–186.
[2] C.N. Hipolito, E. Crabbe, C.M. Badillo, O.C. Zarrabal, M.A.M. Morales, G.P. Flores, M.d.A.C. Hernández, A. Ishizaki, J. Cleaner Prod. 16 (2008) 632–638.
[3] S. Atsumi, T. Hanai, J.C. Liao, Nature 451 (2008) 86–89.
[4] Advanced Research Projects Agency, US Department of Energy. See http://www.energy.gov/news/8207.htm (26.10.09).
[5] A.L.d. Silva, I.L. Muller, Int. J. Hydrogen Energy 36 (2011) 2057–2075.
[6] G.A. Nahar, S.S. Madhani, Int. J. Hydrogen Energy 35 (2010) 98–109.
[7] F. Bimbela, M. Oliva, J. Ruiz, L. Garcıía, J. Arauzo, J. Anal. Appl. Pyrol. 85 (2009) 204–213.
[8] W.J. Wang, Y.Y. Cao, Int. J. Hydrogen Energy 35 (2010) 13280–13289.
[9] W.J. Wang, Fuel 90 (2011) 1681–1688.
[10] W. Wang, Y. Cao, Int. J. Hydrogen Energy 36 (2011) 2887–2895.
[11] R.R. Davda, J.W. Shabaker, G.W. Huber, R.D. Cortright, J.A. Dumesic, Appl. Catal. B 43 (2003) 13–26.
[12] R.D. Cortright, R.R. Davda, J.A. Dumesic, Nature 418 (2002) 964–967.
[13] G.W. Huber, J.W. Shabaker, J.A. Dumesic, Science 300 (2003) 2075–2077.
[14] New York Spot Price, 30th March, 2011.
[15] M.A. Vannice, J. Catal. 50 (1977) 228–236.
[16] J.H. Sinfelt, D.J.C. Yates, J. Catal. 8 (1967) 82–90.
[17] D.C. Grenoble, M.M. Estadt, D.F. Ollis, J. Catal. 67 (1981) 90–102.
[18] E.J. Bosze, J. McKittrick, G.A. Hirata, Mater. Sci. Eng. B 97 (2003) 265–274.
[19] L.G. Jacobsohn, M.W. Blair, S.C. Tornga, L.O. Brown, B.L. Bennett, R.E. Muenchausen, J. Appl. Phys. 104 (2008) 124303.
[20] P. Shuk, H.-D. Wiemhofer, U. Guth, W. Gopel, M. Greenblatt, Solid State Ionics 89 (1996) 179–196.
[21] B. Roy, K. Loganathan, H.N. Pham, A.K. Datye, C.A. Leclerc, Int. J. Hydrogen Energy 35 (2010) 11700–11708.
[22] B. Roy, K. Artyushkova, H.N. Pham, L. Li, U. Martinez, K. Loganathan, A.K. Datye, C.A. Leclerc, in preparation.
[23] G. Wen, Y. Xu, H. Ma, Z. Xu, Z. Tian, Int. J. Hydrogen Energy 33 (2008) 6657–6666.
[24] V. Yu, I.V. Konyukov, V.A. Naumov, Kinet. Catal. 38 (1997) 81–83.
[25] B.C. Michael, A. Donazzi, L.D. Schmidt, J. Catal. 265 (2009) 117–129.
[26] C. Wheeler, A. Jhalani, E.J. Klein, S. Tummala, L.D. Schmidt, J. Catal. 223 (2004) 191–199.
[27] S. Chettibi, R. Wojcieszak, E.H. Boudjennad, J. Belloni, M.M. Bettahar, N. Keghouche, Catal. Today 113 (2006) 157–165.
[28] A. Kambolis, H. Matralis, A. Trovarelli, Ch. Papadopoulou, Appl. Catal. A 377 (2010) 16–26.
[29] Y.H. Hu, E. Ruckenstein, Adv. Catal. 48 (2004) 297–345.
[30] P. Kumar, Y. Sun, R.O. Idem, Energy Fuels 21 (2007) 3113–3123.
[31] T. Zhu, M. Flytzani-Stephanopoulos, Appl. Catal. A 208 (2001) 403–417.
[32] M. Barsoum, Fundamentals of Ceramics, McGraw-Hill Companies Inc, 1997.